Journal of Catalysis 256 (2008) 268–277

Contents lists available at ScienceDirect

Journal of Catalysis

www.elsevier.com/locate/jcat

Hydrogen on polycrystalline β-Ga_2O_3: Surface chemisorption, defect formation, and reactivity

Wilfrid Jochum [a], Simon Penner [a], Karin Föttinger [b], Reinhard Kramer [a], Günther Rupprechter [b], Bernhard Klötzer [a,*]

[a] Institut für Physikalische Chemie, Universität Innsbruck, A-6020 Innsbruck, Austria
[b] Institut für Materialchemie, Technische Universität Wien, Veterinärplatz 1, A-1210 Wien, Austria

ARTICLE INFO

Article history:
Received 7 December 2007
Revised 20 February 2008
Accepted 21 March 2008
Available online 29 April 2008

Keywords:
Gallium oxide
β-Ga_2O_3
Hydrogen adsorption
Defect formation
Thermal desorption spectroscopy
Temperature-programmed reduction
Electric impedance spectroscopy
Infrared spectroscopy

ABSTRACT

The adsorption of H_2 and H_2O on differently pretreated β-Ga_2O_3 samples, exhibiting variable surface chemistry and surface defect concentration, was studied by temperature-programmed reduction, oxidation, and desorption; Fourier transform infrared spectroscopy; and electric impedance measurements. Adsorption of H_2 at 300–473 K resulted in the formation of surface –OH groups with no formation of oxygen defects. Between 473 and 550 K, formation of Ga–H species was observed. At above 550 K, oxygen vacancy/defect formation was observed, resulting in enhanced formation of Ga–H species, accompanied by the formation of more strongly bound Ga–H species. H_2O was observed to quench oxygen vacancies formed by reductive pretreatment and to exhibit a strong hydrolytic affinity to H adsorbed on Ga sites. The effect of water was seen even under strongly reducing conditions (773 K; 1 bar H_2) with only traces of water present.

1. Introduction

Ga_2O_3 is an outstanding material due to its gas-sensing [1,2] and catalytic properties [3–5], and much effort has been focused on the structural, electric and catalytic characterization of different Ga_2O_3 samples [1–8]. The interaction of two important molecules with gallia surfaces, H_2 and H_2O, is attracting increasing interest, because semiconducting Ga_2O_3 thin films are promising sensors for H_2 detection [1,2,9,10] and represent an important catalyst that can catalyze a range of reactions involving breakage or formation of hydrogen-containing bonds (e.g., alkane dehydrogenation and aromatization, methanol synthesis [3,5,11]). From a catalytic standpoint, both the formation and the reactivity of hydrogen adsorbed on Ga_2O_3 are important in the context of hydrogen's potential water–gas shift activity and its activity in methanol synthesis and methanol steam reforming [12,13]. Much of the current knowledge about the interaction of H_2 with different Ga_2O_3 polymorphs originates from the studies of Bonivardi et al. [4,7,14]. Concerning adsorption of H_2, two different types—homolytic dissociative adsorption (i.e., formation of Ga–H species) and heterolytic dissociative adsorption (i.e., formation of Ga–OH and Ga–H species)—have been observed and characterized by in situ FTIR spectroscopy [7]. Regarding the interaction of H_2O with β-Ga_2O_3 surfaces, Meixner et al. [15] examined the co-adsorption of H_2O with different catalytically relevant probe molecules (e.g., H_2 and CO) and found a strong influence of H_2O adsorption (via formation of surface OH groups) on the co-adsorption of other molecules, on the structure of the material itself, and on the catalytically active centers.

Because the surface (defect) chemistry of β-Ga_2O_3 has been identified as the dominant parameter influencing the adsorption properties, here we report a systematic study of the adsorption of H_2 and H_2O on differently pretreated β-Ga_2O_3 samples, which (due to the different treatments) exhibited different surface chemistries and surface defect concentrations. Particular emphasis is given to a precise quantification of the adsorbed molecules by volumetric adsorption measurements.

2. Experimental

2.1. Materials

Two different β-Ga_2O_3 samples were used in this work. First, a commercial low-surface area β-Ga_2O_3 sample (99.99% purity), supplied by Alfa Aesar, was calcined in air at 1000 K. The surface area after pretreatment was determined by nitrogen adsorption at 77 K according to BET as 4.0 m^2/g. Then a high-surface area β-Ga_2O_3 sample was prepared by dissolving the commercial sample in 30% aqueous NaOH, using a PTFE beaker to avoid contamination resulting from glass, followed by dilution with water and precipitation of crystalline $Ga(OH)_3$ at around 363 K, induced by an equimolar

* Corresponding author. Fax: +43 512 507 2925.
E-mail address: bernhard.kloetzer@uibk.ac.at (B. Klötzer).

0021-9517/$ – see front matter
doi:10.1016/j.jcat.2008.03.019

Table 1
Amount of desorbed H_2 determined by TPD peak integration after H_2 pretreatment at the given temperatures, see experimental details given in the caption of Fig. 5

H_2-pretreatment temperature [K]	β-Ga_2O_3 4.0 m^2/g	β-Ga_2O_3 19.4 m^2/g
	H_2-desorption [$\mu mol/m^2$]	H_2-desorption [$\mu mol/m^2$]
373	0.2	0.2
473	0.8	0.5
573	1.4	1.1
673	1.8	1.5
773	1.9	1.6
873	1.8	1.7

amount of ammonium nitrate (with respect to NaOH) in aqueous solution. The precipitate was thoroughly washed with hot deionized water, filtrated, and dried in air at 400 K for 1 h. According to [16], the precipitation of a GaO(OH) containing gel from an aqueous solution, followed by drying and calcination at 673 K, leads to the exclusive formation of α-Ga_2O_3, which can be converted to β-Ga_2O_3 by high-temperature annealing at 1073 K for 4 h. We applied this annealing procedure in air to our sample and obtained a well-ordered β-Ga_2O_3 with a surface area of 19.4 m^2/g. The comparable crystallographic order of both β-Ga_2O_3 samples was confirmed by X-ray diffraction. The "reprecipitated" ~20-m^2/g sample also was evaluated by XPS to estimate the surface-related contaminants; a maximum of $\leqslant$3% Na was found in the near-surface regions, indicating only a limited possible influence of near-surface Na^+ species on the values reported in this work. Differences between the two samples with respect to hydrogen adsorption were rather small. Although the total amount of adsorbed H_2 under the same experimental conditions was very similar (see Table 1), the reducibility of the surface to form vacancies apparently was somewhat lower for the high-surface area sample (see the discussion of Fig. 6 later); however, this also may be due to surface structural differences. Nevertheless, the general trends observed on H_2 adsorption were very comparable.

Hydrogen (5.0), helium (5.0), and oxygen (3.5) were supplied by Messer-Griesheim as high-grade gases. Hydrogen was further purified by passage through an oxygen-removing purifier. Condensable contaminants were removed from hydrogen and helium by liquid nitrogen traps, and oxygen was passed over a trap cooled with liquid nitrogen/ethanol.

2.2. Volumetric apparatus

Volumetric measurements were performed in an all-glass apparatus equipped with metal bellow valves (Witeg), a Baratron pressure transducer (MKS), and mass flow controllers (MKS). To enable volumetric measurements at temperatures of up to 1000 K, the reactor part containing the sample was made of quartz. The mass of the gallia samples was 3.1611 g for the low-surface area sample and 0.9780 g for the high-surface area sample, ensuring sufficient volumetric effects in the measurements.

The Ga_2O_3 samples were treated either in 1 bar flowing dry hydrogen or in 1 bar flowing hydrogen containing a defined water partial pressure, at a typical flow rate of 1.0 ml/s. To control the amount of water, hydrogen was passed through either a U-shaped tube maintained at LN_2 temperature or a reservoir of H_2O maintained at 273 K, leading to a partial water pressure of 6.1 mbar in the gas stream. After hydrogen treatment, the sample was evacuated at 300 K using a diffusion pump (base pressure, 5×10^{-7} mbar) and heated in high vacuum to 973 K at a rate of 10 K/min (TPD measurements), followed by cooling in vacuum to 313 K. The TPO measurements allowed us to study both the rate of the reoxidation process and the total amount of oxygen required for complete reoxidation.

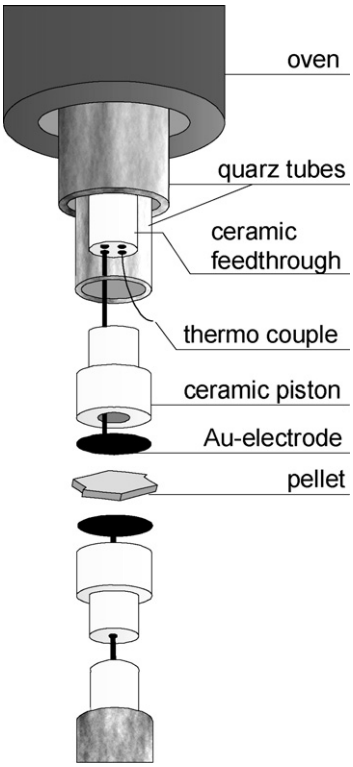

Fig. 1. Scheme of the volumetric apparatus used for the impedance measurements.

2.3. Conductivity apparatus

For impedance measurements, β-Ga_2O_3 (low-surface area sample) was pressed at about 10 kbar for 20 min to produce pellets of about 1.6 mm thickness and 5 mm diameter, using about 100 mg of powder. The electric impedance of the pelletized samples was measured as a function of pretreatment temperature at 1 Hz and a stimulation voltage of 50 mV, using two circular gold electrodes forming a plate capacitor and exerting a pressure of ~1 bar in a vertical quartz tube (Fig. 1). The impedance cell was suited for gas treatments compatible with those applied in the volumetric apparatus. Heating was provided by a tubular oven and controlled by a thermocouple situated in the reactor about 5 mm downstream of the pellet. The temperature was controlled by a thermocouple situated inside the reactor and a Micromega PID temperature controller. The impedance of the sample was determined by a IM6e impedance spectrometer (Zahner-Elektrik), which supplied data on the impedance and the phase angle of the current as a function of voltage (50 mV) in a frequency range of 0.1 mHz to 1 MHz. For both the volumetric and the conductivity measurements, the same procedures were applied for gas supply and cleaning (see above); for both types of experiments, the gases were of highest purity, as supplied by Messer-Griesheim.

2.4. FTIR measurements

FTIR spectra were recorded in transmission mode on a Bruker IFS 28 spectrometer (MCT detector, resolution 4 cm^{-1}). The samples (for IR, the 4-m^2/g Alfa Aesar sample; see above) were pressed into self-supporting wafers (ca. 10 mg) and placed inside a cell with a ring-shaped furnace, which allowed pretreatment in different atmospheres up to 823 K. First, the β-Ga_2O_3 sample was oxidized in a flow of synthetic air at a ramp of 10 K/min up to 823 K, followed by evacuation at this temperature and cooling in vacuum to ca. 10^{-6} mbar. Then reduction was carried out in flowing hydrogen (purified with a liquid nitrogen-cooled trap) at a

heating rate of 5 K/min up to the prespecified final temperature, which was maintained 30 min, followed by cooling in hydrogen flow at a rate of 5 K/min. For the quenching experiments, water was added through a saturator maintained at 273 K (ice/water bath), with the hydrogen flowing through the saturator.

3. Results and discussion

3.1. Volumetric adsorption of H_2

Fig. 2 shows the volumetrically measured H_2 consumption before and during TPR of β-Ga_2O_3 (4.0 m^2/g). Before each TPR experiment, the sample was fully oxidized by a cycle of oxidation in 1 bar flowing O_2 at 973 K for about 1 h, followed by cooling to room temperature in O_2 and then evacuation for >20 min at 313 K. Afterwards, dry hydrogen was admitted at 313 K, leading to an initial amount of adsorbed H_2 of 0.08 μmol/m^2 and an initial H_2 pressure of 95 mbar. The subsequent volumetric TPR experiments involved heating from 313 K to the final temperatures (523, 573, and 973 K) at a rate of 10 K/min, maintaining the maximum temperature for 1 h, and then cooling to 313 K at a rate of 10 K/min.

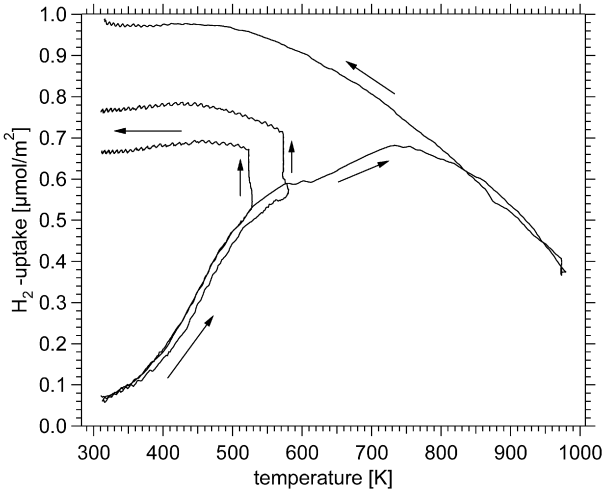

Fig. 2. Volumetric measurement of hydrogen consumption during TPR heating and cooling cycles from 313 K up to maximum temperatures of 523, 573 and 973 K. The initially fully oxidized β-Ga_2O_3 (4.0 m^2/g) was exposed to 95 mbar initial hydrogen equilibrium pressure at 313 K before the ramp was started. Linear heating and cooling rate: 10 K/min.

At temperatures of 313 up to 523 and 573 K, the amount of adsorbed hydrogen increased steeply with temperature. At the respective maximum temperature (maintained for 1 h), some additional hydrogen was irreversibly adsorbed. During cooling, the total amount of hydrogen remained almost constant (at 523 K) or increased only slightly (at 573 K). The experiment at 973 K exhibited analogous behavior during heating up to ~700 K, but beyond 730 K, an onset of hydrogen desorption occurred, as indicated by the reversal of the slope. In the temperature window between 730 and 973 K, the heating and cooling curves almost coincided, suggesting reversibly adsorbed hydrogen, with the amount increasing on cooling. The 730–973 K range of the 973 K experiment can be considered an adsorption isobar, because the total hydrogen pressure remained in the narrow range of 96–100 mbar. During cooling to below 730 K, all of the hydrogen adsorbed at higher temperatures remained on the sample; after cooling to 313 K a total of ~1 μmol of H_2/m^2 was irreversibly consumed.

Based on the foregoing results, we suggest that hydrogen adsorption on β-Ga_2O_3 is an activated process and that the activation barrier was sufficiently high to prevent fully reversible adsorption at temperatures below ~730 K; that is, only above this temperature was a true adsorption equilibrium established with the gas phase. At temperatures below ~600 K, H_2 adsorption is largely a kinetic phenomenon, as suggested by the slow isothermal increase of hydrogen adsorption at 523 and 573 K. As the temperature decreased, the adsorption rate approached zero at around 450 K, where the curves for both 523 and 573 K finally inverted their slopes during cooling, and the total adsorbed amount stagnated

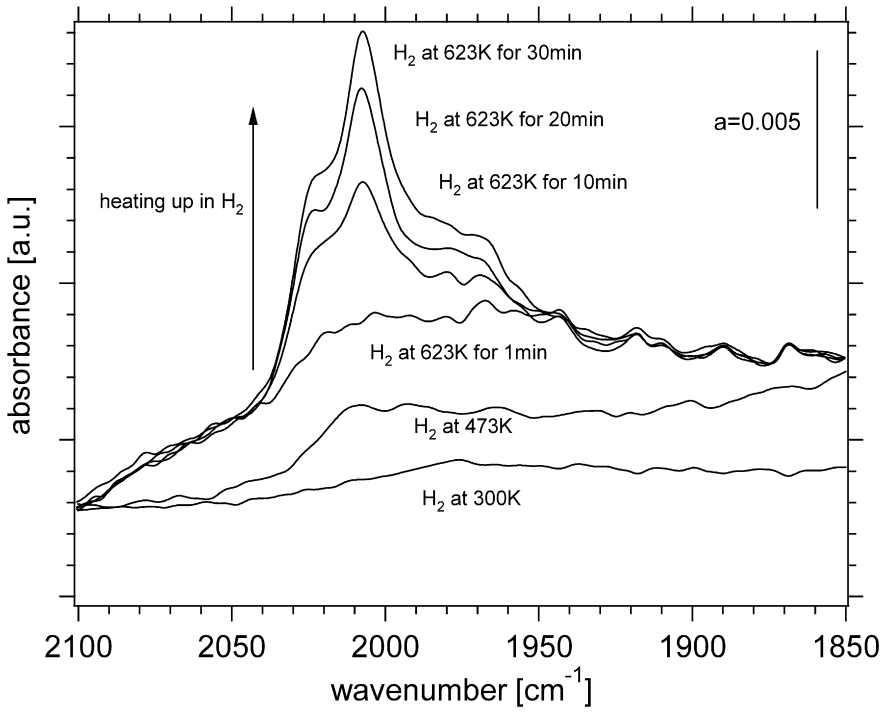

Fig. 3. Infrared spectra (on 4 m^2/g sample) of the 2100–1850-cm^{-1} region during heating up in dry H_2 from room temperature to 623 K and time-resolved at 623 K for 30 min.

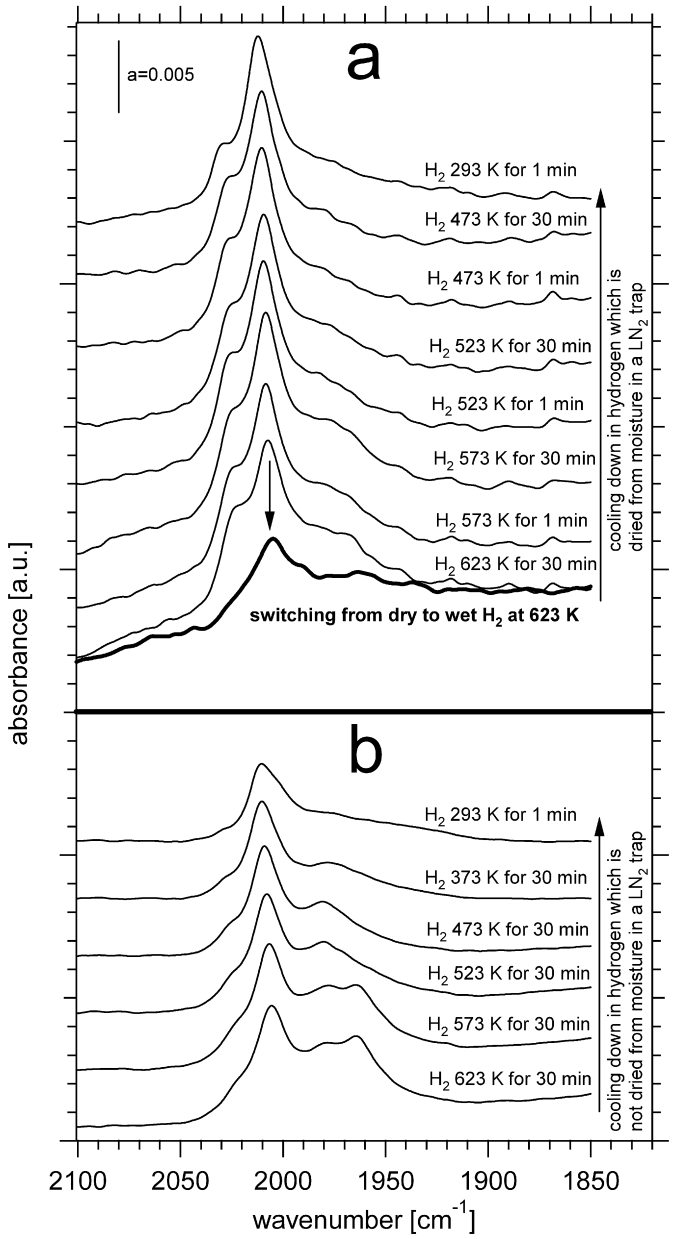

Fig. 4. Infrared spectra (all on 4 m^2/g sample) of the 2100–1850-cm^{-1} region during dry H_2-treatment and cooling down in (a) LN_2-dried H_2 5.0 from 623 to 293 K and decreasing signal after switching from dry H_2 to wet H_2 (6.1 mbar H_2O in 1 bar H_2) at 623 K; (b) cooling down in H_2 5.0 (<5 vpm H_2O, <1 vpm O_2) without LN_2 trap.

at a constant level, depending on the specific sample history. Between 600 and 730 K, a gradual transition from irreversible toward reversible adsorption occurred.

3.2. FTIR results

The TPR measurements allowed us to quantify the amount of adsorbed hydrogen, but we could obtain no information on the specific binding sites of hydrogen (i.e., whether hydrogen is adsorbed on different Ga or O sites). Consequently, we performed IR measurements (Figs. 3 and 4), in close analogy to the volumetric adsorption measurements shown in Fig. 2, to further examine the kinetic behavior observed by TPR below ~730 K. Instead of using static H_2, in these experiments we dosed flowing H_2 onto the fully oxidized Ga_2O_3 sample at 300 K, followed by stepwise heating of the sample up to 623 K and then stepwise cooling back to room temperature. Both conventional H_2 5.0 (impurities, <5 vpm water and <1 vpm oxygen) and H_2 dried over a LN_2 trap (to remove water traces) were used, which proved to be very important for the final result, as we discuss later. The results from the initial heating cycle in LN_2-dried hydrogen 5.0 are shown in Fig. 3. As was found in TPR studies, only a small amount of hydrogen was adsorbed at 300 K (0.08 μmol/m^2 for the low-surface area β-Ga_2O_3). Moreover, the IR spectra of Fig. 3 showed almost no contribution of Ga–H species (expected at around 2010 cm^{-1}) at this temperature. Increasing the reduction temperature to 473 K led to a significant increase in the amount of adsorbed hydrogen in TPR, but only little Ga–H intensity was seen in the IR spectrum (the second spectrum from the bottom in Fig. 3). Raising the reduction temperature to 623 K increased both the total amount of adsorbed hydrogen (TPR) and the number of Ga–H species detected by IR (third spectrum from the bottom). It is noteworthy that for similar reduction temperatures and temperature ranges (i.e., 373–723 K), Bonivardi et al. [7] reported an increase in the Ga–H bands starting at 500 K, paralleled by a decrease in the Ga–OH bands. Thus, we can assume that adsorbed hydrogen gradually shifted to Ga sites at above 500 K.

At this point, it may be useful to consider our summarizing schematic representation of the surface reactions of H_2 and H_2O with the gallia surface in Fig. 9 occurring stepwise at 300–600 K. The upper part of the scheme (except for the top line, which refers to the impedance measurements of thermally induced vacancy formation without H_2 discussed in Section 3.4) illustrates the temperature-dependent transition from homolytically adsorbed H_2 at the initially fully oxygen-terminated surface to heterolytically adsorbed hydrogen and to hydrogen-induced defect formation with homolytical H_2 adsorption at the newly formed cus-Ga sites. The ultimate aim of Fig. 9 is to provide a consistent summary of the results of this work and the literature data on H_2 adsorption on gallia; therefore, we placed this scheme in Section 4.

To further investigate the isothermal kinetic H_2 adsorption observed by TPR, we performed IR experiments under similar experimental conditions, that is, raising the reduction temperature to 623 K and keeping the temperature constant for 30 min in LN_2 dried H_2. IR spectra were then recorded in the Ga–H region every 10 min (see Fig. 3); distinct IR bands were seen at 2025, 2010, 1980, and 1970 cm^{-1}, which can be assigned to different Ga–H vibrations (ν $Ga_{(t)}$–H, ν $Ga_{(o)}$–H, with Ga occupying tetrahedral and octahedral sites, respectively, as outlined in [7]). Comparing the spectra after 10, 20, and 30 min with the spectrum collected after 1 min at 623 K (third spectrum from the bottom) reveals that—in agreement with the TPR experiments—more hydrogen was adsorbed without raising the temperature, and an increasing number of Ga sites were populated, again suggesting a strong kinetic limitation of Ga–H population.

To follow the cooling branch of the TPR outlined in Fig. 2, we performed additional IR measurements, using both LN_2-dried H_2 5.0 (Fig. 4a) and conventional H_2 5.0 (Fig. 4b), to monitor eventual changes in the Ga–H population during cooling and also to assess the influence of gas impurities onto the adsorbed hydrogen species. Therefore, the oxidized Ga_2O_3 sample was heated in flowing H_2 (1 bar) up to 623 K. After maintaining this temperature for 30 min at 623 K (second IR spectrum from the bottom in Fig. 4a; first IR spectrum from the bottom in Fig. 4b), the sample was cooled in dry H_2 in steps to 293 K (third to ninth spectra from the bottom in Fig. 4a; second to third spectra from the bottom in Fig. 4b). Careful analysis of the spectra reveals a much smaller decrease in the intensity of the Ga–H bands as function of temperature in Fig. 4a (a maximum 25% decrease in LN_2-dried H_2), and thus the data of Fig. 4a are in much better agreement with the volumetric measurements shown in Fig. 2. In conventional H_2 5.0, the amount of adsorbed H_2 decreased much more

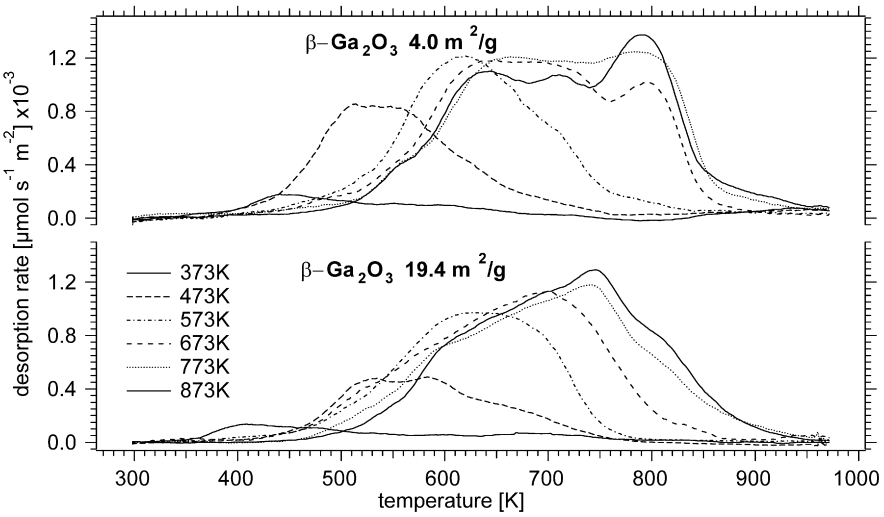

Fig. 5. Temperature programmed hydrogen desorption spectra obtained after heating of both the 19.4 and 4 m^2/g area β-Ga_2O_3 samples from room temperature at +10 K/min to the isothermal reduction temperatures displayed in the graphs, holding at these for 60 min, and followed by cooling down at −10 K/min; all ramp segments were performed in a 60 ml/min flow of 1 bar LN_2-dried H_2. The TPD run was started 30 min after evacuation of the reaction cell.

strongly during cooling (by 46%), and a strong influence of residual gas impurities could be established. To further corroborate the importance of water traces in particular, the sample heated in LN_2-dry flowing H_2 (1 bar) up to 623 K (and maintained there for 30 min, corresponding to the second spectrum from the bottom in Fig. 4a) was switched from dry to wet hydrogen by replacing the LN_2 cold trap by an ice/water mixture, leading to a H_2O partial pressure of 6.1 mbar in the hydrogen feed. This resulted in a strong decrease in the Ga–H intensity (by ∼60%), as shown in the bold spectrum (first from the bottom in Fig. 4a, obtained 1 h after admission of wet H_2). This clearly indicates that water traces efficiently hydrolyzed/removed Ga–H bonds. As mentioned earlier, when dry hydrogen was used, a much smaller intensity drop in the Ga–H IR spectral region was observed, even after the ∼190 min of the entire cooling cycle. Because the LN_2 trap removed the water with high efficiency (but not the oxygen impurities), the residual decrease of 25% after ∼190 min in LN_2-dried H_2 also could be induced by the residual O_2, as well as by residual traces of H_2O being previously present in the in situ IR cell and/or the gas manifold (stainless steel, not bakeable at high temperatures).

Recent studies of hydrogen adsorption on different Ga_2O_3 polymorphs by Collins et al. [7] are mainly at variance with our LN_2-dried H_2 observations. Those authors reported reversible hydrogen adsorption on β-Ga_2O_3 (but also on other gallia modifications) in the temperature range of 323–723 K, and noted that the total equilibrium amount of adsorbed Ga–H increased with increasing temperature but decreased by 43% during cooling in H_2 from 723 to 323 K. They reported that these changes occurred in a reversible fashion, including relatively rapid equilibration of the Ga–H species within several minutes. Accordingly, they proposed a contribution of an H(ads) entropy-driven "endothermal H_2 adsorption equilibrium in one elementary step." But we could observe a comparably strong IR intensity loss during cooling in H_2 only when using conventional hydrogen 5.0 containing some residual moisture, with which we found a decrease of 46% within approximately 210 min. In summary, our IR measurements in dry H_2 strongly corroborate the findings of our TPR experiments, with both demonstrating major differences between heating and cooling.

The Ga–H spectroscopic fingerprints shown in Figs. 4a and 4b exhibit some characteristic changes both during cooling and on deliberate exposition to moisture. Because the shoulder at 2025 cm^{-1} obviously decreased both during cooling and with increasing H_2O content of the hydrogen, the presence and intensity of this shoulder appear to indicate the degree of Ga–H hydrolysis effects. In the presence of conventional H_2 5.0, this feature was hardly visible at 623 K; switching from dry LN_2 to wet H_2 at 623 K also led to a very significant decrease in the intensity of the band at 2025 cm^{-1}. We suggest that the relative intensity loss of this shoulder during cooling in LN_2-dried H_2 is indicative of the residual hydrolysis effects discussed earlier. In summary, we conclude that it is not an easy experimental task to remove all of the residual water quantitatively from the IR cell, but we are happy to have established a clear experimental difference between more and less water-affected experimental observations.

According to the following interpretation of Fig. 5, a stronger population of "strongly binding" cus-Ga–H sites with increasing temperature is likely. These "strongly binding" H(ads) sites will be assigned to Ga centers at vacancies later in our work. After reconsideration, the (exothermal) hydrolysis of these sites, according to the scheme of Fig. 9, would cause a loss of intensity at *higher* wavenumbers, particularly of the shoulder at 2025 cm^{-1}, most likely because these cus-Ga centers at vacancies are hydrolyzed most efficiently. The influence of water traces on the <1980 cm^{-1} region is also obvious from the experiments of Fig. 4, but we cannot provide a plausible assignment of these effects at present.

The concept of "endothermal adsorption in one step" of [7] imposes a general problem if considered up to very high temperatures, because it implies a convergence of the Ga–H surface species to a nonzero constant limiting value at infinite temperatures [with the absolute equilibrium amount of H(ads) depending on adsorption entropy and hydrogen pressure], no matter how high the temperature becomes. According to Fig. 2, the opposite is the case; above ∼730 K, the total hydrogen coverage decreases again. An adsorption equilibrium in the conventional sense is eventually completely shifted toward the gas phase with increasing temperature, which appears to be more likely for temperatures above 730 K.

The situation obviously becomes more complicated in the case of a surface chemical reaction equilibrium involved, if, for example, a defect formation/hydrolysis process is involved. At least in the gallia-hydrogen case, the obvious irreversibility of the low-temperature adsorption process in dry H_2 makes such an one-step endothermal adsorption equilibrium situation unlikely, and the significantly decreased Ga–H intensity during cooling in wet H_2 appears to be largely related to a hydrolysis/reduction equilibrium on the surface, leading to a certain temperature-dependent redistribution of Ga–H(ads) and Ga–OH(ads). A surface reaction equilibrium of this kind can be shifted toward oxygen vacancy formation

with increasing temperature, as has been shown in, for example, [17] for TiO_2. The explanation of our results based on the reaction scheme shown in Fig. 9 in fact involves a reaction step that is very likely endothermic—the process of oxygen vacancy formation from heterolytically adsorbed hydrogen. Thus, it is reasonable to assume that the defect concentration increases with increasing temperature. The cus-Ga sites thus created are efficient centers for (exothermic) homolytic H_2 adsorption (step a1), leading to an increase of Ga–H intensity with increasing temperature, as was observed in all experimental studies up to ∼730 K. Conversely, hydrolytic quenching of these defects, involving the hydrolysis of cus-Ga–H(ads) and partial replacement by O–H species, would be expected to be exothermic, yielding a decrease in Ga–H intensity during cooling.

In principle, the hydrolysis-induced changes on the surface should be at least qualitatively discernible in the OH spectral region. Unfortunately, the OH region appeared as an uncharacteristic broad, rather high-intensity band at around 3500 cm^{-1} [ν(GaO–H)], particularly under H_2 equilibrium pressure, and demonstrated no distinct spectroscopic features assignable to, for example, specific OH groups involved in the hydrolysis reaction. The main problem in interpreting the OH region is the same as in reported previously [7]; the observed relative intensity variations at different temperatures in both dry and wet H_2 were rather weak. Qualitatively, the coexistence of Ga–OH and Ga–H groups from heterolytic H_2 adsorption at around 700–300 K can be extracted from our IR data (OH region not shown, for reasons stated above) and from [7], indicating that a certain amount of Ga–H species was always populated under equilibrium H_2 pressure, not exclusively limited to the cus-Ga sites for homolytic H_2 adsorption (see the scheme in Fig. 9) but present over the entire surface. Thus, the heterolytic H_2 adsorption could induce much OH background. In fact, on initial adsorption, the low-temperature region (470–570 K) exhibited both Ga–H and OH intensity in parallel, although in this range, vacancies/cus-Ga sites can be excluded by our TPO measurements, and thus "normal" heterolytic adsorption of H_2 in the absence of cus-Ga sites appears highly likely, as outlined in our model. In our opinion, how much of the OH intensity actually comes from the H_2 surface adsorption- or reaction-induced processes, from "conventional" surface hydroxylation through heterolytic water dissociation or from other background effects, cannot be readily determined.

3.3. Temperature-programmed desorption results

The effect of the hydrogen reduction temperature on the formation of specific surface species and oxygen vacancies was further studied by TPD. Fig. 5 shows two series of TPD spectra obtained after H_2 reduction of fully oxidized (oxidation in 1 bar dry O_2 at 973 K for 1 h) β-Ga_2O_3 samples of differing specific surface areas. The hydrogen reduction/adsorption cycle involved heating from 300 K to the reduction temperature at a rate of 10 K/min and in a constant flow of 60 ml/min dry H_2 (1 bar), maintaining the sample in the H_2 flow at the final reduction temperature for 1 h, and then cooling to 300 K in H_2. Before the TPD spectrum was obtained, the sample was maintained for around 30 min under high vacuum (∼3×10^{-6} mbar) at 300 K.

Table 1 presents the amount of H_2 desorbed (deduced from Fig. 5) in μmol/m^2. Although the surface area of the two samples differed by a factor of 5, the hydrogen uptake per m^2 was nearly the same, indicating that the hydrogen uptake was confined to the surface. A rough estimation of the number of surface-binding sites on β-Ga_2O_3 can be obtained by calculating the average number of "Ga_2O_3" centers within 1 cm^2 of the average β-Ga_2O_3 surface. Based on the molecular weight and the density of the solid, the molar volume of β-Ga_2O_3 of 31.9 cm^3/mol can be derived (i.e., 1 cm^3 contains 0.0313 mol or 1.89×10^{22} stoichiometric units of Ga_2O_3). Taking the power of 2/3 of this number, we arrived at an estimate of 7.09×10^{14} units/cm^2 = 11.8 μmol/m^2. Assuming that $Ga^{\delta+}$–$O^{\delta-}$ units are necessary for the heterolytic binding of one dissociated H_2-molecule, the average β-Ga_2O_3 surface was found to contain ∼23.6 μmol/m^2 adsorption sites. The maximum amount observed in our experiments was 1.9 μmol/m^2 H_2, corresponding to a mean coverage of $\Theta = 0.08$. This low coverage indicates that the H_2 adsorption most likely is a defect-related phenomenon.

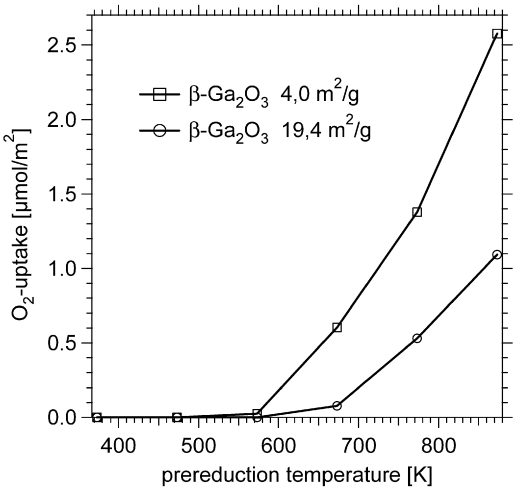

Fig. 6. Whole O_2-reuptake after reduction with H_2 and H_2-TPD measurements on the 4.0 and 19.4 m^2/g β-Ga_2O_3 samples.

Fig. 5 also demonstrates that the nature of the hydrogen adsorption sites depends strongly on the reduction conditions. If the H_2 pretreatment was performed below 573 K, the H_2 desorption peak maximum exhibited a pronounced shift toward lower temperatures both for the high-surface area (19.4 m^2/g) and low-surface area (4 m^2/g) samples. Higher reduction temperatures (see Fig. 5) led to a progressive increase in stronger hydrogen binding sites (desorption maxima shifted up to 800 K) and, in parallel, a decrease in weaker binding sites. This observation, together with the finding of activated H_2 adsorption (see Figs. 2 and 3), suggests that the strong binding sites were essentially formed during H_2 exposure, and that their amount increased significantly at $T_{red} > 573$ K.

Some hints as to the possible nature of these (newly formed and removed) binding sites are available. The desorption peak component at the highest temperatures (700–800 K) is clearly associated with the formation of near-surface oxygen vacancies, as we discuss later in the context of Fig. 6.

At this point, we should consider some electronic, rather than structural, analogies between gallium oxide and zinc oxide. ZnO is known to adsorb hydrogen heterolytically on around 5–10% of its surface sites [18]. We observed ca. 8% on β-Ga_2O_3. Obviously, Zn^{2+} and Ga^{3+} are isoelectronic species, both with the electronic configuration [Ar]$3d^{10}$. Differences originate from the slightly higher nuclear charge of Ga^{3+} and an average 1.5-fold higher coordination number with respect to lattice oxygen in a different geometry. Two distinct adsorption processes have been observed for ZnO, using calorimetry and other methods [19,20]: (preferential) homolytic H_2 adsorption at low coverage on polar surfaces and heterolytic adsorption on nonpolar surfaces. The topic "heterolytic versus homolytic H_2 adsorption on ZnO" has been addressed in a number of experimental and theoretical studies [21,22] that found a stronger heterolytic bonding (O^{2-}–H^+ and Zn^{2+}–H^-) and a weaker homolytic binding of H_2, preferentially as two O^{2-}–H^* bonds. Obviously, polar surfaces (which tend to exhibit oxygen termination for the fully oxidized surface) are likely candidates for preferential homolytic $2H^*$ bonding at specific surface oxygen centers. The

IR study by Collins et al. [7] provided evidence that a similar situation may apply to various surfaces of polycrystalline Ga_2O_3 polymorphs. When fully oxidized Ga_2O_3 was exposed to H_2 below ~500 K (yielding TPD spectra characteristic of weakly adsorbed H_2; see Fig. 5), the IR spectra exhibited increased Ga–OH intensity, and a significant population of Ga–H species was not observed, especially during the first heating cycle. When reduction was performed above ~500 K, the Ga–OH species became progressively weaker and the Ga–H intensity increased. Higher H_2 reduction temperatures created more and more coordinatively unsaturated ("cus-") Ga sites, due to increasing surface reduction/oxygen defect formation. In the temperature range 298–550 K, no oxygen vacancies were produced, but a marked shift of the TPD peak maxima toward higher temperatures still occurred, along with an increasing contribution of Ga–H species in the IR spectra (see Fig. 3). Most likely, the least-activated adsorption process (dominant up to 473 K) was homolytic hydrogen adsorption on terminal oxygen sites (leading to more weakly adsorbed hydrogen desorbing at lower temperature), followed by heterolytic H_2 adsorption without defect formation as the next step (at 473–573 K) and finally oxygen vacancy formation and stronger hydrogen binding at these sites at temperatures above 573 K (cf. the reaction scheme shown in Fig. 9).

3.4. O_2 and H_2O adsorption on reduced β-Ga_2O_3

In an alternative route for studying defect formation in dry H_2, the O_2 uptake after different hydrogen reduction treatments was measured (Fig. 6). Below 550 K, H_2 was adsorbed (cf. Fig. 5), but no O_2 uptake was observed after complete H_2 desorption (heating in high vacuum to 973 K), indicating that no oxygen defects were formed. Defect formation in dry H_2 occurred only at temperatures above 550 K (Fig. 6). For example, the defect concentration induced by exposure to 1 bar dry H_2 at 873 K was 1.1–2.6 μmol O_2/m^2 depending on the sample, whereas at 573 K, almost no defects were generated on either sample.

A clear difference between the low- and high-surface area samples was the degree of near-surface structural defects, in addition to their differing Na content. It would be highly unlikely for both samples to have exactly the same concentration of structural low-coordination sites/defects. The oxygen vacancy concentrations (see Fig. 6) will not directly scale with the total hydrogen coverage if the hydrogen is distributed differently between oxygen vacancy-related cus-Ga adsorption sites (formed at the high temperatures) and other "normal" sites. The TPD series shown in Fig. 5 indicates that the hydrogen distribution with respect to strong binding sites was not identical on both samples. In particular, the desorption component at 800 K, most likely strongly bound H(ads) at oxygen vacancies, was underrepresented on the high-surface area sample, obviously because less vacancies were available, as can be derived from Fig. 6. Whether the differences in surface reducibility are due to chemical (Na) or to structural differences between the surfaces is not clear at this time.

Nevertheless, more vacancies (cus-Ga sites) led to more strongly bonded H(ads) in the TPD spectra (~800 K region). On reduction at 573 K (Fig. 6; high- and low-surface area Ga_2O_3), no vacancies were generated, but at 873 K, the vacancy concentration (measured by O_2 uptake after H(ads) removal) was, for example, 2.2 μmol/m^2 (Fig. 6; 2×1.1 μmol/m^2 O_2 uptake, high-surface area sample). The additional adsorbed amount of H(ads) at 873 K relative to the amount at 573 K was 2×0.6 μmol $H_2 = 1.2$ μmol H(ads) per m^2, again on the high-surface area sample. This means that sufficient vacancy-related cus-Ga sites were available after the reduction at 873 K for the more strongly bonded extra hydrogen. We note that this estimate is at the limits of accuracy of our measurements, and that the oxygen vacancies possibly could have been quantitatively blocked by H(ads) after high-temperature reduction and cooling in dry H_2. Consequently, it is quite likely that the successive population of the ~800 K TPD component in Fig. 5 quantitatively scales with the additional formation of oxygen vacancies or cus-Ga sites at temperatures above 550 K.

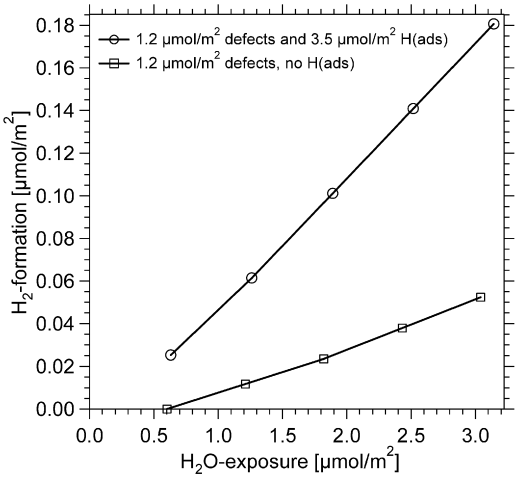

Fig. 7. Reactivity of oxygen defects with preadsorbed hydrogen and without preadsorbed hydrogen toward water at 313 K on the low-surface β-Ga_2O_3 sample (4.0 m^2/g); reduction at 673 K in flowing dry H_2 for 1 h leads to 1.2 μmol/m^2 O-defects and 3.5 μmol/m^2 H adsorbed. Squares: reduction at 673 K, again in flowing dry H_2, for 1 h and removal of H(ads): 1.2 μmol/m^2 defects. H_2O adsorption at 313 K: H_2-formation and partial reoxidation at 313 K; circles: reduction at 673 K for 1 h and cooling down in flowing dry H_2 to 313 K leads to 3.5 μmol/m^2 H(ads) preadsorbed and 1.2 μmol/m^2 O-defects. H_2O adsorption induces H_2-formation and partial reoxidation at 313 K.

As described in detail previously, H_2O has a strong affinity to Ga–H sites and thus reduces the number of Ga–H species in favor of Ga–OH species. Thus, we studied the interaction of H_2O with both H(ads) and defects generated by H_2 reduction. The sample was reduced in dry H_2 at 773 K for 1 h, yielding 1.2 μmol/m^2 oxygen vacancies (Fig. 6), and then the feed gas was switched from dry to wet H_2 (i.e., 6.1 mbar H_2O in 1 bar H_2) at 773 K. This treatment led to complete reoxidation of Ga_2O_3, indicating that H_2O was able to fully quench surface-related oxygen vacancies, even when only traces of water were present under strongly reducing conditions (1 bar H_2). The complete reoxidation by water quenching was verified by the following procedure: switching from dry to wet H_2 (6.1 mbar H_2O in 1 bar H_2 at 773 K for 60 min), high-vacuum (10^{-6} mbar) pumping at 773 K for 10 min, heating in high vacuum at a rate of 10 K/min to 973 K to remove H(ads) quantitatively (see Fig. 5), cooling under high-vacuum conditions at −10 K/min to 313 K, volumetric oxidation of the vacancies by O_2 first at room temperature, and, for full oxidation, TPO up to 973 K at a rate of 10 K/min.

As outlined earlier, oxygen vacancies (cus-Ga sites) can be created by reduction in flowing dry H_2 at above 573 K and can be obtained in an "H-adsorbate-free" state by subsequent thermal desorption of H_2 up to 973 K in vacuo. The amount of such prepared adsorbate-free vacancies can be quantified by reproducible TPO measurements using O_2.

To quantify the reaction of water with these adsorbate-free oxygen vacancies after complete hydrogen desorption, as well as the reaction with H(ads) remaining on the sample after the same reduction, the experiment in Fig. 7 was performed with low-surface area β-Ga_2O_3. Two types of samples with the same defect concentration (1.2 μmol/m^2 of O defects, prepared by H_2 reduction at 673 K for 1 h), but with and without H(ads) (removed by H_2-TPD), were exposed to repeated doses of 0.6 μmol H_2O/m^2 Ga_2O_3. After each exposure, the total pressure change and the change in the

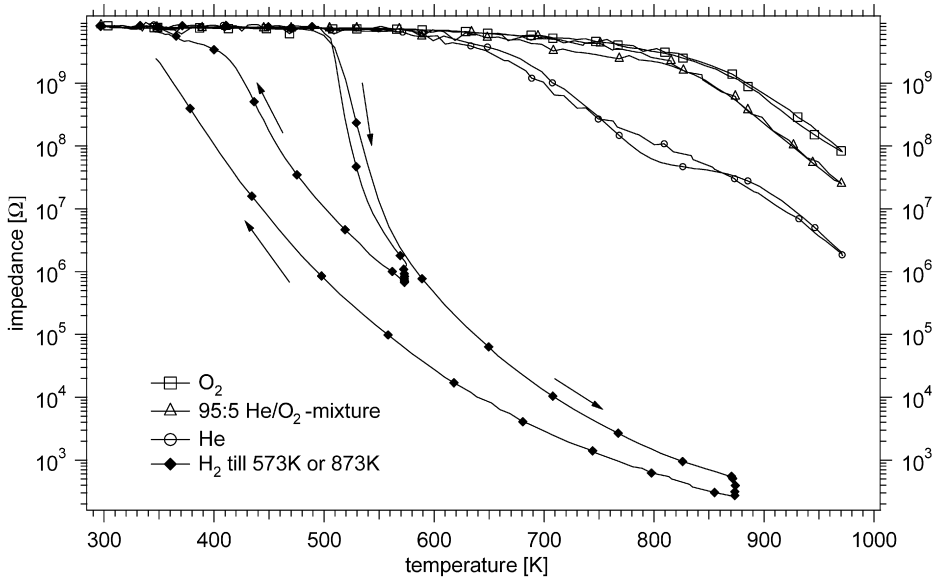

Fig. 8. In situ impedance measurements on 4.0 m^2/g surface sample measured at 1 Hz. Before each measurement: oxidation with dry O_2 at 973 K for about 1h. Heating ramp +5 K/min and cooling ramp −5 K/min; in H_2 1 h at the maximum temperatures; 10 min at the maximum temperatures for all other measurements. Open squares: 1 bar O_2, measurement in flowing dry O_2 (1 ml/s); triangles: 95:5 flowing He/O_2-mixture (1 ml/s); open circles: clean, dry He; filled rhombs: 1 bar dry H_2 till 573 or 873 K, respectively.

gas composition in the TPR cell were determined. For the sample with defects but without preadsorbed hydrogen, no hydrogen production was observed on exposure to 0.6 µmol H_2O/m^2 Ga_2O_3; thus, it is reasonable to assume that, at least in the beginning, H_2O adsorbed heterolytically on an oxygen vacancy by forming –OH and an additional Ga–H species, but with no H_2(g) production. If more H_2O was admitted (1.2 µmol H_2O/m^2 Ga_2O_3), then the newly formed Ga–H species were at least partially hydrolyzed to Ga–OH species, and ∼0.01 µmol of gaseous H_2/m^2 Ga_2O_3 was formed after the second water dosage. After a sequence of consecutive water dosages, a linear dependence of H_2 production on total H_2O exposure was observed in the chosen exposure range.

In contrast, when H_2O was exposed to a sample that initially exhibited both oxygen defects (1.2 µmol O defects/m^2 Ga_2O_3) as well as H(ads) [i.e., 3.5 µmol H (ads)/m^2 Ga_2O_3; that is, Ga–H species were present initially], the Ga–H species were replaced by Ga–OH even at very low H_2O exposure (e.g., on exposure to 0.6 µmol of H_2O/m^2 Ga_2O_3, 0.03 µmol of H_2/m^2 Ga_2O_3 was formed). This experiment again demonstrated a linear dependence of H_2 production on H_2O exposure, but importantly, the slope was now more than twice as steep as that resulting from the H(ads)-depleted defective samples.

As demonstrated by the lower part of the reaction scheme shown in Fig. 9, in principle two H_2 molecules can be formed for each hydrogen-covered oxygen vacancy (and some surplus H_2 from hydrolysis of Ga–H from the "conventional" heterolytic Ga–H species), whereas only one H_2 molecule can be formed when preadsorbed H is absent. But because only a fraction of the exposed water was converted to H_2 in both cases, most of the H_2O remained physisorbed. In summary, it is easy to quench the defects with water and also to hydrolyze the Ga–H species. In the presence of large amounts of water, both the defects and the adsorbed Ga-hydrogen species will be removed and replaced by surface OH groups.

3.5. Electric impedance spectroscopy results

Ga_2O_3 is a purely *n*-conducting oxidic semiconductor that can act as an efficient chemical sensor due to its gas-dependent and temperature-dependent electric conductivity (a topic most relevant to sensoring physics). The basic features of the thermally and chemically induced conductivity of gallia are summarized in [23] and the references therein. Consequently, we complemented our experiments with electric impedance measurements obtained under the experimental conditions (i.e., temperature ranges) similar to those examined by TPR, TPD, and IR. Fig. 8 displays temperature-dependent impedance spectra measured in various gas feeds (at 1 Hz and a stimulation voltage of 50 mV). In clean, dry oxygen (open squares in Fig. 8), the impedance decreased only above 700 K (the resulting charge carriers are considered to be electrons situated in intergap sites), because above this temperature, the equilibrium between lattice oxygen decomposition/defect formation and molecular O_2(g) became increasingly shifted toward the gas phase:

$$2O^{2-} \rightleftarrows O_2 + 4e^- + 2\#.$$

When the oxygen partial pressure was reduced to ∼50 mbar (open triangles), the impedance at a given temperature was somewhat lower than that in dry O_2, because the lower partial pressure of O_2 shifted the aforementioned equilibrium to the right, producing an increased amount of charge carriers at any given temperature. In a flow of dry He, the impedance decreased more significantly with temperature, due to the very low partial pressure of O_2 (∼5 ppm O_2 impurities, but no H_2 impurities specified on the He 5.0 cylinder). Apparently, even this tiny oxygen partial pressure was sufficient for reversible reoxidation of the defects during cooling, because hardly any hysteresis was observed.

A much more effective pathway for defect formation was reduction in clean and dry H_2 performed in two temperature-programmed experiments up to 573 or 873 K (see the filled rhombs in Fig. 8). In both TPR experiments, the impedance began to decrease at temperatures above 510 K in dry flowing H_2 (1 bar). Below 510 K, a considerable amount of H(ads) was present on the surface (see Fig. 2), but no impedance decrease was observed during heating, probably because hydrogen adsorbed without defect formation on top of already existing sites (largely homolytic H_2 adsorption on oxygen-terminated surfaces and increasing heterolytic adsorption as Ga–H above 473 K; see Fig. 3). From Fig. 6, we concluded (by TPO) that "chemically" measurable defects were formed at temperatures above 550 K, and that mainly surface-adsorbed

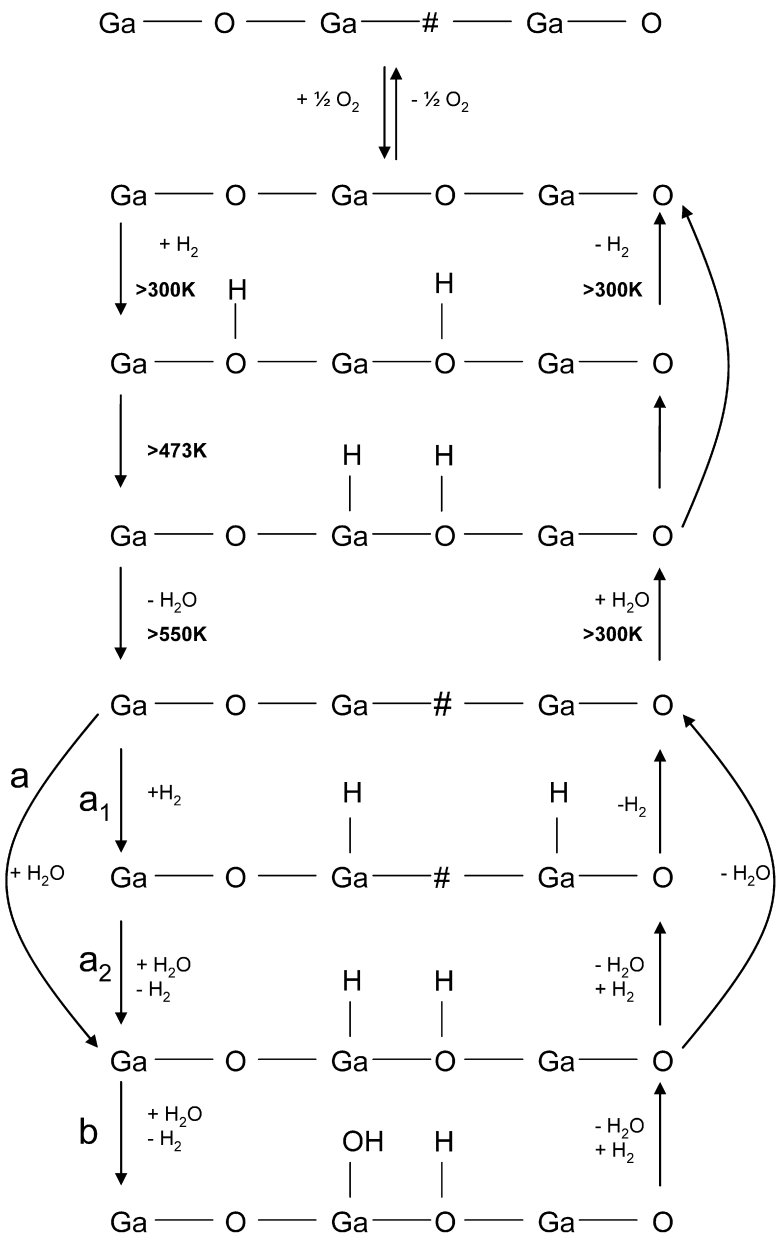

Fig. 9. Scheme of H_2 and H_2O adsorption as well as defect formation on β-Ga_2O_3.

H(ads) was present at temperatures below 550 K. Because the H_2-induced impedance changed by more than 3 orders of magnitude between 510 and 550 K (see Fig. 8), the conductivity measurement appeared to be much more sensitive than titration by O_2 to minute numbers of defects. We can conclude that initial defect formation, which is inevitably linked to the formation of additional Ga–H bonds, started at above 510 K, but that chemically relevant defect concentrations were attained at above 550 K. However, the IR results of Fig. 3 suggest an onset of Ga–H formation at around 473 K. The question remains as to whether Ga–H species can be formed on specific sites between 473 and 510 K that are not situated adjacent to oxygen vacancies and do not contribute to conductivity, for example, heterolytically adsorbed hydrogen without surface oxygen removal in the form of water.

During cooling from 573 K, an almost constant hydrogen surface concentration of ∼1.4 μmol/m^2 can be assumed, as can be deduced from Fig. 5 and indicated in Table 1. This means that it is not the chemical state of the surface, but rather the thermal availability of the charge, that induces changes during cooling from 573 to below 400 K. An Arrhenius plot of the 573–440 K cooling data exhibited perfect linear behavior, and a thermal charge carrier activation energy of ∼1.1 eV was estimated.

A similar impedance behavior was observed after H_2 treatment up to 873 K. Beyond 573 K, the additional strong impedance decrease was caused by additional O vacancy formation and hydrogen adsorption (see Fig. 6 and Table 1 for quantification). At 873 K, the formation of 5.1 μmol/m^2 of O defects could be deduced, a number that remained constant during cooling in dry hydrogen. According to Fig. 2, during cooling from 973 K, the hydrogen coverage changed only between 973 and ∼600 K; it remained almost constant at lower temperatures, and the activation energy for thermal charge carriers on the “constant vacancy–constant hydrogen coverage” sample was the same as that in the run at 573 K (i.e., ∼1 eV). The lower total impedance of the sample treated at 873 K versus that treated at 573 K during cooling simply reflects the greater number of defects and the greater hydrogen coverage induced by the reduction at 873 K. Nonetheless, the thermal activation energy for this larger number of carriers was almost the

same as that obtained from the experiment conducted at 573 K. We conclude that the total number of charge carriers determines the total impedance (i.e., more defects with more adsorbed hydrogen correspond to a higher carrier concentration), but that their thermal activation barrier does not strongly depend on either defect or hydrogen concentration.

Compared with Fig. 2, hysteresis of the impedance traces at 573 and 873 K nicely corroborates the volumetric adsorption hysteresis shown in Fig. 2 at the same temperature range. Comparing our IR results (see Fig. 3) with those of Collins et al. [7] corroborates the initial population of mostly oxygen-terminated adsorption centers, and thus it is reasonable to infer that any H_2 adsorbed below 510 K did not lead to thermally excitable charge carrier formation. Once Ga–H bonds were formed at defects above 510 K, a sudden onset of conductivity was observed.

Summarizing the impedance measurements, defect formation and electric conductivity can be caused by direct desorption of lattice oxygen and—most effectively—by surface/lattice oxygen reduction in H_2. Hydrogen-covered defects induce maximum conductivity, providing the maximum number of charge carriers. Their thermal activation requires ∼1 eV. From the lattice oxygen desorption process without hydrogen, an apparent activation barrier of ∼2.2 eV was deduced in the temperature range 860–973 K; however, in this case a superposition of the shift of the aforementioned chemical equilibrium and the true thermal activation barrier of the charge carriers must be considered.

4. Conclusion

Combining results of TPR, TPO, and TPD with IR and impedance spectroscopy, a schematic model of defect formation and hydrogen–water interaction with β-Ga_2O_3 can be suggested, as depicted in Fig. 9. The fully oxidized surface is in thermal equilibrium with an oxygen-deficient structure prepared by heating in O_2, depending on O_2 pressure and temperature (e.g. in 1 bar O_2, defect formation began at around 700 K).

With H_2 at above room temperature, homolytic H_2 adsorption on the initially available terminal oxygen species occurred mainly through formation of surface –OH groups at up to 473 K. Significant formation of Ga–H species (which do not induce measurable electric conductivity) began at 473 K, but on a largely vacancy-free surface. Above 510–550 K (depending on the method used), formation of oxygen vacancies, which contribute thermally excitable electrons, occurred through H_2O abstraction, a reversible step. In dry H_2, hydrogen loss from cus-Ga–H sites was significantly diminished with decreasing temperature, as indicated by the IR experiments. The temperature of quantitative H_2 desorption was found to be dependent on the (pre)reduction temperature. Adsorption of hydrogen on the oxygen-deficient surface resulted in a predominant formation of cus-Ga–H species (step a_1). Subsequent adsorption of H_2O partially quenched the oxygen vacancies through the formation of surface –OH groups and H_2 (step a_2). Further H_2O adsorption led to the formation of Ga–OH species and additional release of H_2 (step b); that is, H_2O adsorption with preadsorbed H(ads) resulted in the formation of two H_2's per oxygen vacancy. In contrast, for H_2O adsorption without preadsorbed H (step a followed by step b), only one H_2 per oxygen vacancy was formed. All of the reaction steps discussed herein appear to be largely reversible, except the reformation of the more weakly bonded "homolytic H(ads)" at the fully oxygen-terminated surface, which instead represents a kinetic intermediate toward heterolytic H_2 adsorption.

References

[1] T. Weh, J. Frank, M. Fleischer, H. Meixner, Sens. Actuators 78 (2001) 202.
[2] A. Trinchi, W. Wlodarski, Y.X. Li, Sens. Actuators B 100 (2004) 94.
[3] Y. Ono, Catal. Rev. Sci. Eng. 34 (1992) 179.
[4] S.E. Collins, M.L. Baltanas, J.L. Garcia Fierro, A.L. Bonivardi, J. Catal. 211 (2002) 252.
[5] G.D. Meitzner, E. Iglesia, J.E. Baumgartner, E.S. Huang, J. Catal. 140 (1993) 209.
[6] S. Penner, B. Klötzer, B. Jenewein, F. Klauser, X. Liu, E. Bertel, Thin Solid Films (2007), doi: 10.1016/j.tsf.2007.08.094, in press.
[7] S.E. Collins, M.A. Baltanas, A.L. Bonivardi, Langmuir 21 (2005) 962.
[8] M. Yamaga, E.G. Villora, K. Shimamura, N. Ichinose, M. Honda, Phys. Rev. B 68 (2003) 155207.
[9] M. Fleischer, H. Meixner, Sens. Actuators B 6 (1992) 257.
[10] R. Pohle, M. Fleischer, H. Meixner, Sens. Actuators B 68 (2000) 151.
[11] I. Takahara, M. Saito, M. Inaba, K. Murata, Catal. Lett. 96 (2004) 29.
[12] A.L. Bonivardi, D.L. Chiavassa, C. Querini, M.A. Baltanas, Stud. Surf. Sci. Catal. 130D (2000) 3747.
[13] N. Iwasa, T. Mayanagi, N. Ogawa, K. Sakata, N. Takezawa, Catal. Lett. 54 (1998) 119.
[14] E.A. Gonzalez, P.V. Jasen, A. Juan, S.E. Collins, M.A. Baltanas, A.L. Bonivardi, Surf. Sci. 575 (2005) 171.
[15] F. Reti, M. Fleischer, H. Meixner, J. Giber, Sens. Actuators B 18–19 (1994) 138.
[16] M.R. Delgado, C.O. Arean, Z. Anorg. Allg. Chem. 631 (2005) 2115.
[17] H. Haerudin, S. Bertel, R. Kramer, J. Chem. Soc. Faraday Trans. 94 (10) (1998) 1481.
[18] R.J. Kokes, Acc. Chem. Res. 6 (1973) 226.
[19] L. Zhou, Y. Grillet, J. Rouquerol, Chin. Sci. Bull. 41 (2) (1996) 173.
[20] C. Wöll, Prog. Surf. Sci. 82 (2007) 55.
[21] R.P. Eischens, W.A. Pliskin, M.J.D. Low, J. Catal. 1 (1962) 180.
[22] A.B. Anderson, J.A. Nichols, J. Am. Chem. Soc. 108 (1986) 4742.
[23] M. Fleischer, H. Meixner, J. Appl. Phys. 74 (1) (1993) 300.